












Observation of optical feedback dynamics in single-mode terahertz quantum cascade lasers: Transient instabilities

Xiaoqiong Qi ¹, Karl Bertling ¹, Thomas Taimre ², Gary Agnew ¹, Yah Leng Lim ¹, Tim Gillespie,¹ Ashley Robinson,^{3,1} Michael Brünig ¹, Aleksandar Demić,⁴ Paul Dean ⁴, Lian He Li,⁴ Edmund H. Linfield ⁴, A. Giles Davies ⁴, Dragan Indjin ⁴ and Aleksandar D. Rakić ^{1,*}

¹*School of Information Technology and Electrical Engineering, The University of Queensland, Brisbane, QLD 4072, Australia*

²*School of Mathematics and Physics, The University of Queensland, Brisbane, QLD 4072, Australia*

³*L3Harris Micro Pty Ltd., 7 Hi-Tech Court, Brisbane Technology Park, Eight Mile Plains, QLD 4113, Australia*

⁴*School of Electronic and Electrical Engineering, University of Leeds, Leeds LS2 9JT, United Kingdom*



(Received 25 October 2020; revised 9 December 2020; accepted 11 February 2021; published 8 March 2021)

We provide an experimental evidence of transient instabilities (TIs) in a terahertz (THz) quantum cascade laser (QCL) under optical feedback, in contrast to the widely accepted claim that THz QCLs are ultrastable against feedback. The TIs appear as periodic oscillations in emitted power or terminal voltage of the laser with an increasing oscillation frequency as feedback increases. The absence of relaxation oscillations and low linewidth enhancement factor in THz QCLs makes them a platform uniquely suitable for exploring external-cavity-related dynamics in semiconductor lasers. This work opens a pathway to a THz sensing and imaging modality based on these TIs, which has much reduced complexity compared to existing approaches using laser feedback interferometry.

DOI: [10.1103/PhysRevA.103.033504](https://doi.org/10.1103/PhysRevA.103.033504)

I. INTRODUCTION

Semiconductor lasers experiencing delayed reinjection of emitted power from an external reflector can exhibit a great variety of dynamic behavior. This behavior can differ markedly between different laser types. In particular, optical feedback (OF) dynamics in laser diodes (LDs) are complicated due to the competition between the relaxation oscillation frequency, f_{RO} , and the external cavity resonant frequency, $f_{EC} = c/(2n_{ext}L_{ext})$, where c is the speed of light in a vacuum, and n_{ext} and L_{ext} are the refractive index and length of the external cavity, respectively. In the long cavity regime when $f_{RO} \gg f_{EC}$, the Tkach and Chraplyvy diagram identified five feedback regimes [1–3], while in the short cavity regime when $f_{RO} < f_{EC}$, different self-organizing dynamics from chaotic dynamics take place, such as periodic pulsing at f_{EC} [4] and regular pulse packages [5]. OF dynamics in terahertz (THz) quantum cascade lasers (QCLs) are significantly simplified due to the absence of relaxation oscillations [6]. This effectively removes one dimension contributing to the OF dynamics in THz QCLs. In addition, the low linewidth enhancement factor of THz QCLs further reduces coupling from phase to amplitude [6], which makes THz QCLs a platform uniquely suitable for exploring external-cavity-related OF dynamics in semiconductor lasers.

Laser dynamics and instabilities in QCLs under OF have been extensively studied in the past few years [3,6–12]. However, existing work has focused largely on midinfrared (MIR)

QCLs, which typically have a significantly larger linewidth enhancement factor than that of THz QCLs. This difference markedly affects the laser dynamics. Focusing on steady-state instabilities, Columbo *et al.* found very interesting mode-switching dynamics and regular or irregular dynamics in a MIR QCL with OF [7]. But it was concluded that THz QCLs are ultrastable under any OF levels due to the low value of the linewidth enhancement factor [6,7]. The feedback regimes for a MIR QCL were also experimentally investigated, and five feedback regimes corresponding to the regimes defined for an LD were found [8].

The literature on OF dynamics in THz QCLs is sparse, with frequency instabilities being studied; see, e.g., Ref. [12]. That work explored the frequency instability of the signal from a pair of THz QCLs, whereby it is not possible to attribute spectral changes to just one of the pair. Therefore the impact of OF on a single THz QCL remains unexplored.

In this work we demonstrate experimentally and provide the theoretical explanation for the transient instabilities (TIs) in a THz QCL. We demonstrate that the TIs we observed originate from the beating between the single laser cavity mode and external cavity modes (ECMs) and appear as periodic oscillations in emission power and terminal voltage of the THz QCL experiencing OF. We further quantify OF conditions impacting the TI wave form and demonstrate the frequency modulation properties of the TIs. These TIs have particular relevance to QCLs operating in pulsed mode with pulse duration on the order of hundreds of nanoseconds [13] because they will appear as perturbations within each pulse. The frequencies of the TIs are primarily determined by the external cavity length which provides a pathway for THz sensing and imaging modality with much reduced complexity [14].

*Corresponding author: a.rakic@uq.edu.au

II. THEORETICAL MODEL AND SIMULATION RESULTS

A. Reduced rate equation model

Figure 1 depicts a schematic of a single-mode THz QCL under OF. The laser beam, which is linearly polarized, is collimated using a Tsurupica plastic lens with 30-mm focal length, and OF strength is controlled with a polarizer. The OF dynamics could be observed by monitoring the fluctuations

$$\frac{dS(t)}{dt} = MG[N_3(t) - N_2(t)]S(t) + \frac{M\beta_{sp}N_3(t)}{\tau_{sp}} - \frac{S(t)}{\tau_p} + \frac{2\kappa}{\tau_{in}}\sqrt{S(t)S(t - \tau_{ext})} \cos[\omega_{th}\tau_{ext} + \phi(t) - \phi(t - \tau_{ext})], \quad (1)$$

$$\frac{d\phi(t)}{dt} = \frac{\alpha}{2} \left(MG[N_3(t) - N_2(t)] - \frac{1}{\tau_p} \right) - \frac{\kappa}{\tau_{in}} \sqrt{\frac{S(t - \tau_{ext})}{S(t)}} \sin[\omega_{th}\tau_{ext} + \phi(t) - \phi(t - \tau_{ext})], \quad (2)$$

$$\frac{dN_3(t)}{dt} = \frac{\eta_3}{q} I(t) - G[N_3(t) - N_2(t)]S(t) - \frac{N_3(t)}{\tau_3}, \quad (3)$$

$$\frac{dN_2(t)}{dt} = \frac{\eta_2}{q} I(t) + G[N_3(t) - N_2(t)]S(t) + \frac{N_3(t)}{\tau_{32}} + \frac{N_3(t)}{\tau_{sp}} - \frac{N_2(t)}{\tau_{21}}, \quad (4)$$

where $S(t)$ and $\phi(t)$ are the photon population and the phase of the electric field, respectively, while $N_3(t)$ and $N_2(t)$ represent the carrier populations in the upper and lower laser levels (ULL/LLL) of the active cavity. Once the equations are solved, the time traces of the emission output power can be calculated by $P_{out}(t) = \eta_0 \hbar \omega S(t) / \tau_p$, where $\eta_0 = a_m / 2(a_{total})$ is the power output coupling coefficient, where $a_m = \ln(R_2)^{-1} / L_{in}$ is the mirror loss of the laser cavity and a_{total} is the total loss in the laser cavity, including the mirror loss and waveguide loss. The meaning and value of the other parameters are summarized in Table I if not described elsewhere. The input parameters in the RREs were determined from first principles as described in Ref. [15].

B. Transient instabilities in the emission power

Figure 2(a) depicts simulated time traces of the emission power $P_{out}(t)$ from the THz QCL under increasing feedback coupling coefficient κ for L_{ext} of 0.8 m. The corresponding laser emission spectra offset from the emission frequency (2.752 THz) $P_{out}(\nu)$ (obtained by performing Fourier transform of the slowly varying envelope of the electric field $\sqrt{P_{out}(t)} \exp[j\phi(t)]$ over the period 0–500 ns) is shown in Fig. 2(b). In the free-running state (i.e., no OF), lasing starts after a short turn-on delay (around hundreds of picoseconds) due to ultrashort carrier lifetimes in QCLs. The emission spec-

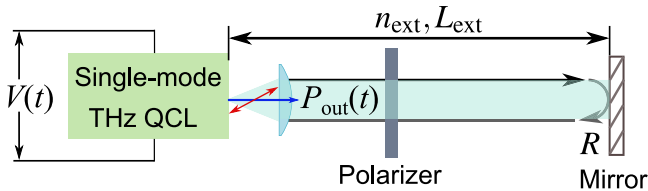


FIG. 1. Schematic of a THz QCL under OF, where n_{ext} and L_{ext} are the refractive index and length of the external cavity, respectively, and R is the reflectivity of the mirror. $P_{out}(t)$ and $V(t)$ are the emission power and the terminal voltage of the single-mode THz QCL, respectively.

trum exhibits a single mode at the emission frequency 2.752 THz (i.e., at 0 in the offset spectrum). In the presence of OF, the emission power starts varying and gradually exhibits peri-

The set of single-mode RREs with OF terms for a THz QCL are as follows:

TABLE I. Parameters used in Eqs. (1)–(5).

Parameter	Value
η_3 —Injection efficiency into ULL	54.41%
η_2 —Injection efficiency into LLL	1.65%
I —Drive current	1.2 A
τ_3 —Total carrier lifetime in ULL	5.0×10^{-12} s
τ_{32} —Nonradiative relaxation time from ULL to LLL	1.76×10^{-10} s
τ_2 —Total carrier lifetime in LLL	2.1×10^{-11} s
τ_{sp} —Spontaneous emission lifetime	1.0×10^{-6} s
τ_p —Photon lifetime	9.02×10^{-12} s
G —Gain factor per period	$2.3 \times 10^4 / 90 \text{ s}^{-1}$
M —Number of periods in active cavity	90
β_{sp} —Spontaneous emission factor	1.627×10^{-4}
ω_{th} —Emission frequency with no OF	1.73×10^{13} rad/s
L_{ext} —External cavity length	0.8 m
n_{ext} —Refractive index of external cavity	1.00
τ_{ext} —Round-trip time of the external cavity, $\tau_{ext} = 2L_{ext}n_{ext}/c$	5.34×10^{-9} s
L_{in} —Laser cavity length	2 mm
n_{in} —Refractive index of active region	3.3
τ_{in} —Round-trip time of laser cavity, $\tau_{in} = 2L_{in}n_{in}/c$	4.403×10^{-11} s
κ —Feedback coupling coefficient, $\kappa = \epsilon \sqrt{R/R_2}(1 - R_2)$	Varies
ϵ —Re-injection coupling factor	Varies
R —Reflectivity of external mirror	0.7
R_2 —Reflection coefficient of laser facet	0.2861
α —Linewidth enhancement factor	−0.1
C —Feedback parameter, $C = \kappa \tau_{ext} \sqrt{1 + \alpha^2} / \tau_{in}$	Varies
q —Elementary charge	1.602×10^{-19} C
c —Speed of light in vacuum	299792458 m s ^{−1}

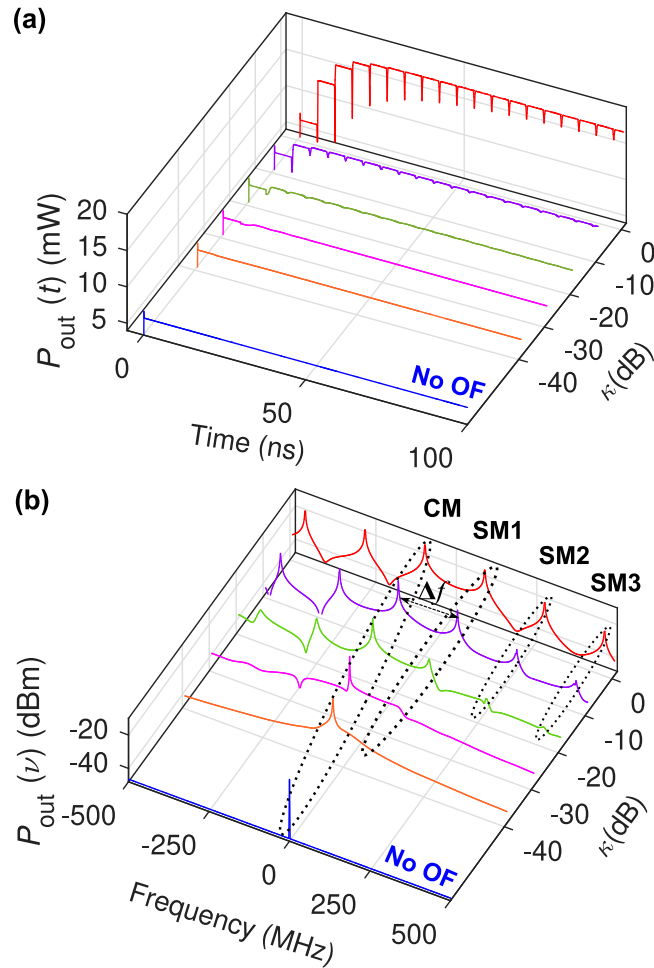


FIG. 2. Simulated (a) time traces of the emitted power from the THz QCL $P_{\text{out}}(t)$ and (b) emission spectra offset from the single-mode frequency at 2.752 THz $P_{\text{out}}(\nu)$ at varying feedback coupling coefficient κ with L_{ext} of 0.8 m and α of -0.1 , where the blue curves show the results with no OF. The changes of the locations of the central mode (CM), first side mode (SM) (SM1), second SM (SM2), and third SM (SM3) are grouped by dashed circles, respectively, in the emission spectra. The mode spacing between the adjacent modes is equal and is defined as Δf .

odic oscillations and even pulses separated by short intervals (around round-trip time of the external cavity length τ_{ext}) that are reducing with κ [Fig. 2(a)]. Accordingly, frequency splitting from the central-mode (CM) to side-mode (SM) ECMs, with the number of SMs and mode spacing Δf increasing with κ is obtained [Fig. 2(b)]. It is confirmed in this work that no chaotic oscillations were observed from the THz QCL under OF when the reinjection coupling factor ε varies from -40 to 0 dB (κ varies from -39.04 to 0.96 dB), within which region conventional LD is dominated by chaotic oscillations. The results shown above correspond to the THz QCL with parameters from the design of Barbieri *et al.* [16]. We have also observed the same phenomenon using the parameters from the Wienold *et al.* design [17]. This clearly shows that this phenomenon, observed in models for two very different THz QCL classes, is not specific to a particular design. In addition, we only considered the dominant optical feedback

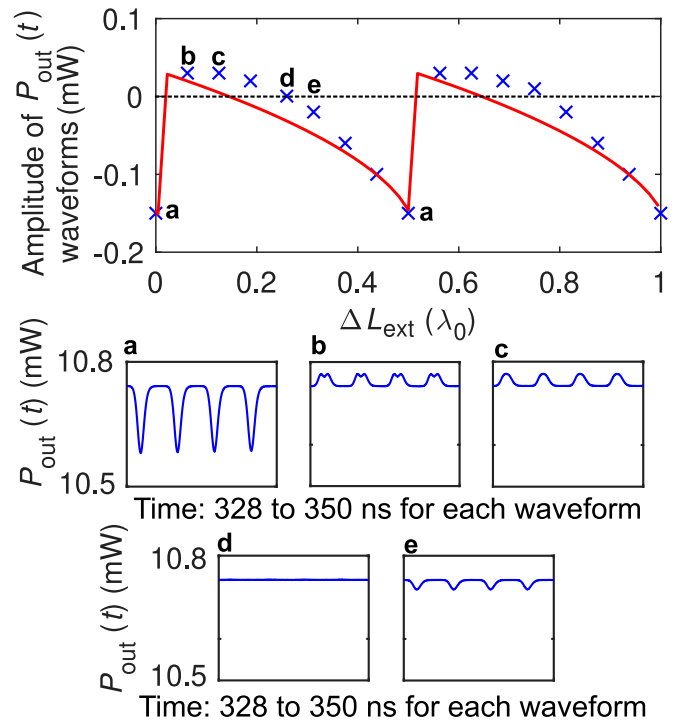


FIG. 3. Simulated amplitude of the emission power wave forms at 350 ns as a function of ΔL_{ext} from 0.8 m with $\kappa = -4.0$ dB (blue crosses), which has a similar trend of the self-mixing wave form obtained from solving the excess phase equation with the same value of κ (red curve). Typical wave form of $P_{\text{out}}(t)$ along ΔL_{ext} at points a, b, c, d, e are also shown in inset a, b, c, d, e, respectively.

term from the first external cavity round trip in the RREs, while the TIs would likely be enhanced quantitatively by involving multiple external cavity round trips, perhaps with additional side modes appearing in the feedback spectrum.

C. Dynamic wave forms in the emission power

Interestingly the pulse wave form of $P_{\text{out}}(t)$ under strong feedback depends on the feedback phase. Figure 3 shows the simulated amplitude of $P_{\text{out}}(t)$ wave forms while varying the external cavity length by an amount ΔL_{ext} from 0.8 m. At each ΔL_{ext} for a fixed $\kappa = -4.0$ dB, wave forms were obtained from $P_{\text{out}}(t)$ by solving RREs, and the amplitudes of $P_{\text{out}}(t)$ wave forms were obtained at the nearest peak at around 350 ns (blue crosses in Fig. 3). This amplitude changes from -0.15 to 0.01 mW with the period of a half wavelength, which is similar to the self-mixing wave forms obtained by solving the excess phase equation [18] at the same κ (red curve in Fig. 3). The existence of the positive (pointing up) and the negative (pointing down) peaks indicates that the emitted power can be increased or decreased depending on the feedback phase [insets of Figs. 3(a)–3(e)]. It is interesting to find a two-peak pulse wave form at point b, which is close to the solution jump region (coexistence of multiple solutions) of the excess phase equation. By plotting the line with amplitude of 0, we find the wave form at point d (as shown in inset d) has a significantly reduced amplitude ($0.5 \mu\text{W}$) when ΔL_{ext} is $0.2594 \lambda_0$. These wave forms repeat by each $\lambda_0/2$, which corresponds to a length of λ_0 for the external cavity round trip.

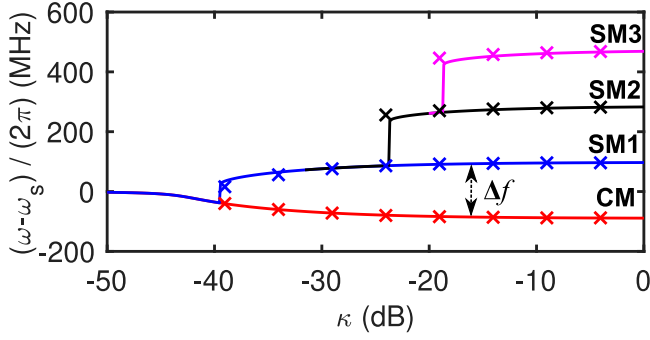


FIG. 4. Simulated mode frequency splitting from CM (red) to adjacent SM1 (blue), SM2 (black), and SM3 (magenta) with the OF level κ . The crosses indicate the results from solving RREs, while the solid curves are the results from the excess frequency equation.

D. Frequency splitting and shifts in the transient instabilities

Figure 2(b) shows that both the CM and SMs exhibit frequency shifts with κ . This can be explained by the excess frequency equation, which describes the steady-state variation of the emission frequency of a semiconductor laser (including LDs and QCLs) due to OF:

$$\omega - \omega_s = -\frac{\kappa}{\tau_{in}} \sqrt{1 + \alpha^2} \sin(\omega\tau_{ext} + \arctan \alpha). \quad (5)$$

Equation (5) indicates that the frequency shift of the emission frequency depends on the feedback coupling coefficient κ , round-trip time of the internal laser cavity τ_{in} , linewidth enhancement factor α , frequency ω , and round-trip time of the external cavity τ_{ext} . Therefore, for a laser feedback system with fixed structure, i.e., fixed τ_{in} and τ_{ext} , if we assume a constant α , the frequency shift is determined only by the mode frequency ω and the feedback coupling coefficient κ .

By solving Eq. (5) with increasing orders of the solutions developed from the algorithm described in [19], Fig. 4 depicts frequency splitting from the CM (red) to the adjacent first SM (SM1, blue) and subsequent second SM (SM2, black) and third SM (SM3, magenta), and the variation of each mode frequency $[(\omega - \omega_s)/(2\pi)]$ with the OF level κ . The crosses indicate results obtained by solving RREs. It is observed that the CM has a redshift with κ while all SMs have blueshifts with κ . As shown in Fig. 4, whether the shift is red or blue is determined by the sign of $\omega - \omega_s$ [left-hand side of Eq. (5)], which is in turn determined by the sign of the sinusoidal function in the right-hand side of Eq. (5) when the values of the current mode frequency ω_s , τ_{in} , τ_{ext} , and α are substituted into the function. This results in reducing pulse intervals and increasing Δf with growing κ in Figs. 2(a) and 2(b), respectively.

The dependence of the mode spacing Δf on κ obtained from solving RREs (crosses) and the excess frequency equation (solid lines) are shown for different values of L_{ext} in Fig. 5(a) with $\alpha = -0.1$. The red, blue, and black curves indicate Δf when L_{ext} is 0.8, 1.6, and 3.2 m, respectively. It is observed that Δf increases with rising κ and saturates at the external cavity resonant frequency f_{EC} under the highest feedback level (100% OF: $\varepsilon = 1$ and $\kappa = 0.96$ dB) for each L_{ext} . The value of f_{EC} is 187.4, 93.7, and 46.8 MHz, respec-

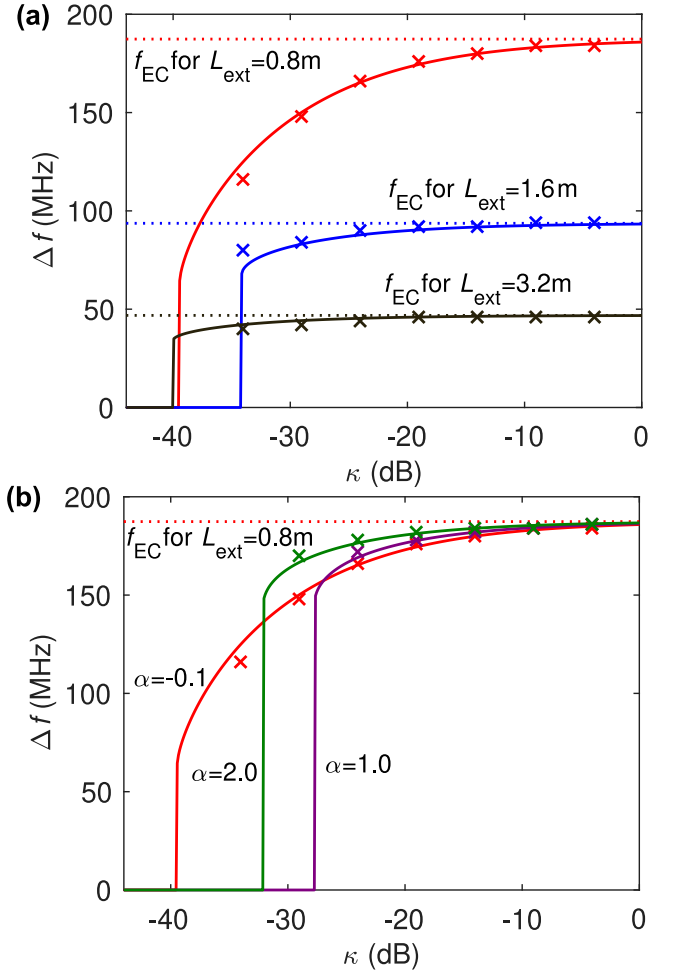


FIG. 5. Simulated mode spacing Δf as a function of κ for (a) $L_{ext} = 0.8$ m (red crosses and curve), 1.6 m (blue crosses and curve), and 3.2 m (black crosses and curve) where $\alpha = -0.1$; and for (b) $\alpha = -0.1$ (red crosses and curve), 1.0 (purple crosses and curve), and 2.0 (green crosses and curve), where $L_{ext} = 0.8$ m. The crosses indicate results from solving the RREs, while the solid curves are the results from the excess frequency equation. Dashed lines indicate the external cavity resonant frequencies f_{EC} for each L_{ext} .

tively, when L_{ext} is 0.8, 1.6, and 3.2 m, as indicated by dashed red, blue, and black lines in Fig. 5(a). Further, it was found that when L_{ext} is fixed, although Δf is different for varying α at each OF level κ , eventually it will saturate at the same value of f_{EC} . As shown in Fig. 5(b), Δf for α of -0.1 , 1.0, and 2.0 all converged to 187.4 MHz with a fixed L_{ext} of 0.8 m. The value of κ at which SM1 splits off from CM predicted from the excess frequency equation varies for different values of L_{ext} and α . This nonmonotonic behavior is determined by the nonlinear nature of the excess phase equation. The dependence of the mode spacing Δf (the oscillation frequency of the feedback dynamics) on the feedback level κ in a THz QCL could be used to estimate the value of the reinjection coupling coefficient, the reflection coefficient of the target or the laser facet, and the linewidth enhancement factor if other parameters are known.

In order to show the dependence of Δf on both L_{ext} and κ simultaneously, we calculate Δf by solving RREs for a

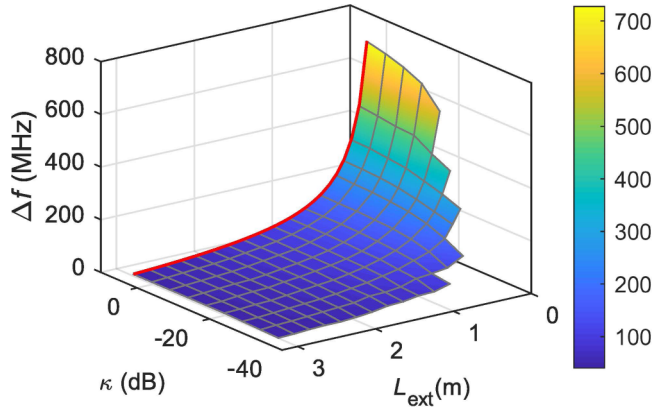


FIG. 6. Simulated dependence of Δf on L_{ext} and κ with $\alpha = -0.1$, where L_{ext} is varying from 0.2 to 3.2 m and κ is varying from -39.04 to 0.96 dB. The color bar indicates the value of Δf (MHz). The red curve indicates $f_{\text{EC}} = c/(2n_{\text{ext}}L_{\text{ext}})$ for varying L_{ext} , which matches very well with simulated Δf by solving RREs at varying L_{ext} with the strongest OF ($\kappa = -0.96$ dB).

varying L_{ext} from 0.2 to 3.2 m with a step length of 0.1 m if $0.2 \text{ m} < L_{\text{ext}} < 0.6 \text{ m}$ and of 0.2 m for $0.6 \text{ m} < L_{\text{ext}} < 3.2 \text{ m}$, and for each L_{ext} we vary κ from -39.04 to 0.96 dB. The result is shown in Fig. 6. It can be observed that under the highest feedback level (100% OF: $\varepsilon = 1$ and $\kappa = 0.96$ dB), Δf matches very well with the f_{EC} , as marked by the red curve in Fig. 6. For shorter L_{ext} with higher f_{EC} , the frequency modulation property is much clearer than that with longer L_{ext} . When L_{ext} is shorter than 0.5 m, due to the corresponding smaller value of C (as defined in the Table I), ECMs appear under stronger OF strength. For example, when L_{ext} is 0.2 m, clear frequency splitting is not observed until κ is -19.04 dB. It was observed from simulation that the TIs appear under moderate and strong OF conditions with $C \geq 1$, which is consistent with the condition of frequency splitting in LDs [2].

A critical value that determines the stability of OF dynamics in THz QCLs is the linewidth enhancement factor α . Figures 7(a) and 7(b) depict simulated $P_{\text{out}}(t)$ and $P_{\text{out}}(\nu)$ from a hypothetical QCL with $\kappa = -4.0$ dB and $\alpha = -0.1, 1, 2, 3$, and 4, respectively. It was observed that $P_{\text{out}}(t)$ gradually dissipates when $\alpha = -0.1, 1$, and 2. However, stable periodic oscillations transit to quasichotic oscillations at around 375 ns when $\alpha = 3$. And this transition occurs earlier (at around 170 ns) when $\alpha = 4$. A broadened and quasicontinuous emission spectrum is obtained in this case. Therefore, increasing α can enhance the laser instability from transient dynamics to stable persistence of multimode emission.

III. EXPERIMENTAL RESULTS

Experimentally, the variations in the laser terminal voltage were monitored directly without using photodetectors. Since the emission power and terminal voltage of the THz QCL are determined by the photon population and the carrier population in the active region, respectively, the feedback dynamics obtained from the emission power and terminal voltage are directly proportional to one another (due to the nature of stimulated emission) [18]. The THz QCL used in this work consisted of a 12 μm -thick GaAs/AlGaAs nine-

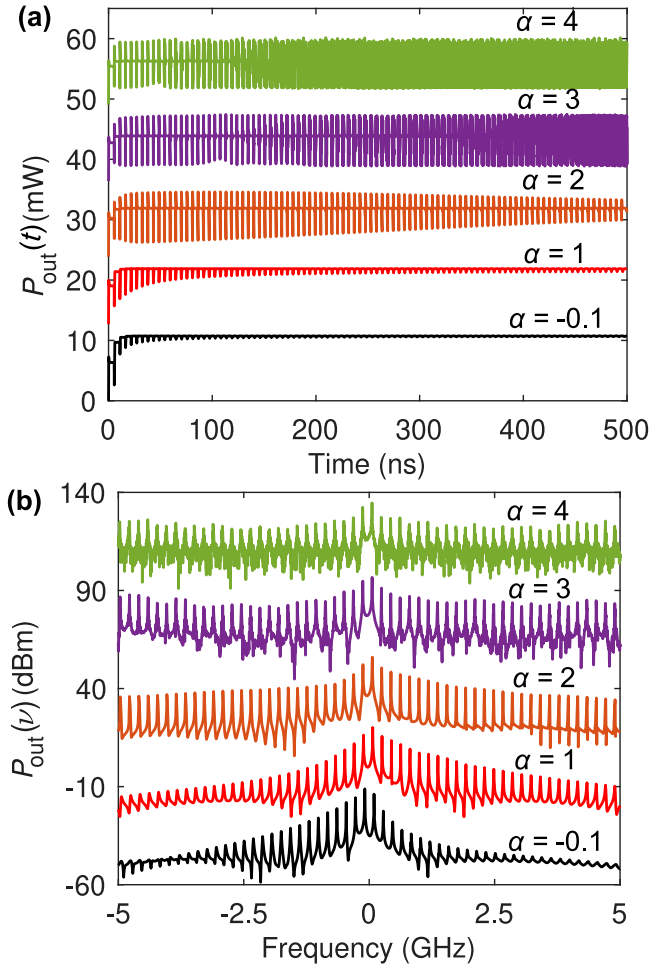


FIG. 7. Simulated dependence of OF dynamics on α with $\kappa = -4.0$ dB: (a) time traces of $P_{\text{out}}(t)$ for a hypothetical QCL with $\alpha = -0.1, 1, 2, 3$, and 4; (b) the corresponding emission spectrum offset to the emission frequency $P_{\text{out}}(\nu)$ with $\alpha = -0.1, 1, 2, 3$, and 4. The results are offset for clarity, the vertical values can only be used for relative variance comparisons.

well phonon-assisted active region and with the fabrication process described in [13]. Experimentally observed TIs in a pulse-mode THz QCL operating at 50 K are shown in Fig. 8. The driving current was set as a square pulse train with a pulse duration of 500 ns and 10% duty cycle. Pulses were trimmed by adjusting the rising time, and the terminal voltage of the laser $V(t)$ was extracted as described in [13]. Since we calibrated $V(t)$ by removing the reference trace from the QCL with no OF, all the peculiarities of pulsed operation, which include the impedance mismatch (parasitic effects), have been removed from the extracted voltage. In addition, as thermal effects are around 100 times slower than the TIs observed here, the difference in time scales rules out the influence of thermal effect on the observed results [15,20]. Figures 8(a), 8(b) and 8(c) depict time traces (left column) and corresponding spectra (right column) of $V(t)$ dynamics for L_{ext} of 0.8, 1.0, and 1.5 m, respectively. In Fig. 8(a) the results are with an increasing OF strength when the round-trip transmission through the polarizer was set at -2.68 dB (orange), -1.58 dB (magenta), and -1.38 dB (blue), respectively. It is observed

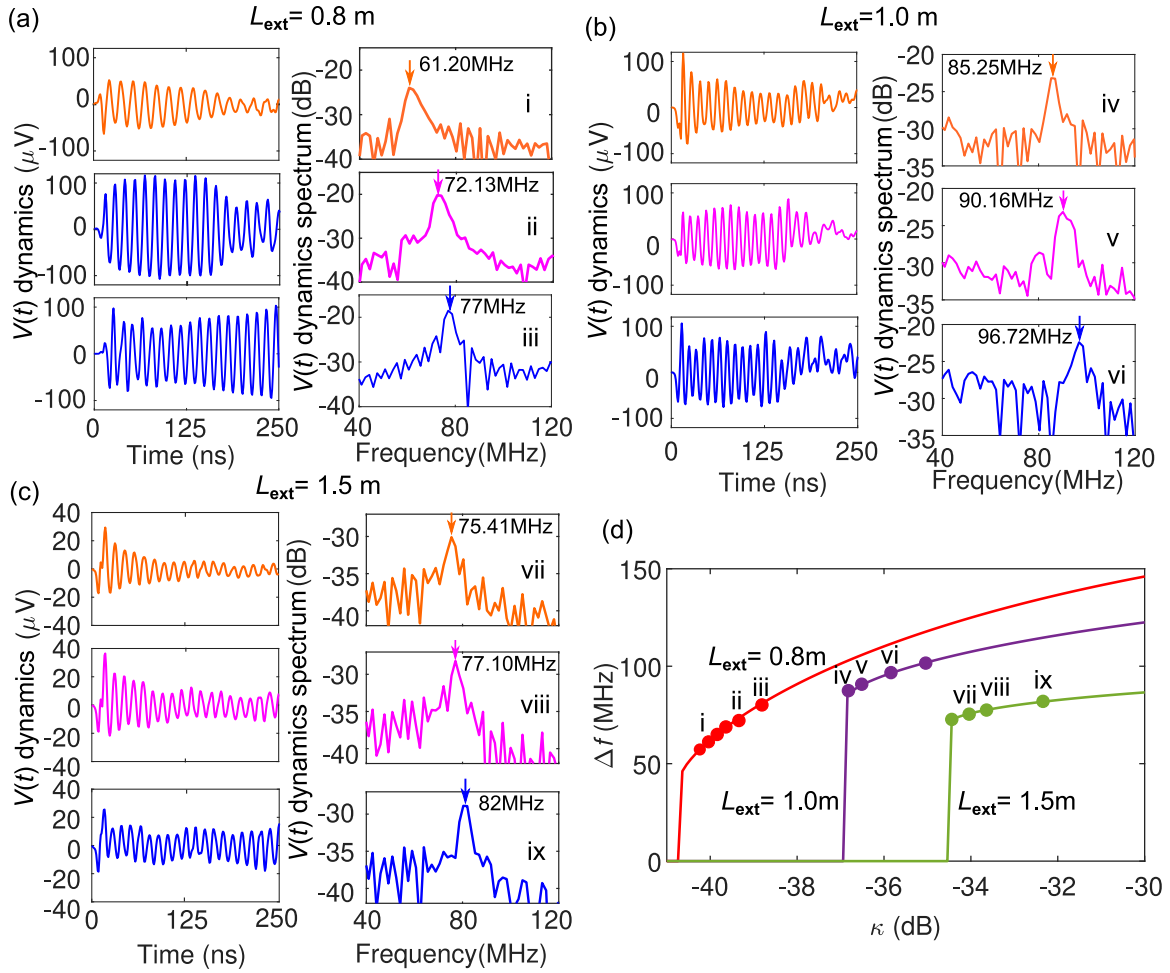


FIG. 8. Experimentally observed time traces of TIs (left column) and corresponding spectra (right column) in a pulse-mode THz QCL when (a) $L_{\text{ext}} = 0.8$ m, with an increasing OF strength when the round-trip transmission through the polarizer was set at -2.68 dB (orange), -1.58 dB (magenta), and -1.38 dB (blue), respectively; (b) $L_{\text{ext}} = 1.0$ m, with an increasing OF strength when the round-trip transmission through the polarizer was set at -7.68 dB (orange), -7.32 dB (magenta), and -6.63 dB (blue), respectively; (c) $L_{\text{ext}} = 1.5$ m, with an increasing OF strength when the round-trip transmission through the polarizer was set at -2.50 dB (orange), -1.71 dB (magenta), and -0.5 dB (blue), respectively; (d) simulated oscillation frequency Δf as a function of κ with $\alpha = -0.0001$ for $L_{\text{ext}} = 0.8$ m, 1.0 m, and 1.5 m. The peak frequencies in (a) correspond to red dots at points i, ii, and iii when $L_{\text{ext}} = 0.8$ m. The peak frequencies in (b) correspond to purple dots at points iv, v, and vi when $L_{\text{ext}} = 1.0$ m. The peak frequencies in (c) correspond to green dots at points vii, viii, and ix when $L_{\text{ext}} = 1.5$ m.

that the oscillation amplitude increases and dissipates over a longer time period with increasing OF strength. The fundamental frequencies of the oscillations are found to be 61.20, 72.13, and 77.0 MHz with increasing OF strength, as indicated by the peak frequencies in the corresponding spectra. We can find the corresponding κ for these oscillation frequencies as -40.24 , -39.24 , and -39.04 dB, respectively, from the simulation result shown in Fig. 8(d) with $L_{\text{ext}} = 0.8$ m and $\alpha = -0.0001$, as indicated by the red dots at points i, ii, and iii. In Fig. 8(b) the results are with an increasing OF strength when the round-trip transmission through the polarizer was set at -7.68 dB (orange), -7.32 dB (magenta), and -6.63 dB (blue), respectively. The corresponding oscillation frequencies are 85.25, 90.16, and 96.72 MHz, which are marked by purple dots at points iv, v, and vi in Fig. 8(d) with $L_{\text{ext}} = 1.0$ m. In Fig. 8(c) the results are with an increasing OF strength when the round-trip transmission through the polarizer was set at -2.50 dB (orange), -1.71 dB (magenta), and -0.5 dB (blue),

respectively. The corresponding oscillation frequencies are 75.41, 77.10, and 82.0 MHz, which are marked by green dots at points vii, viii, and ix in Fig. 8(d) with $L_{\text{ext}} = 1.5$ m. Although further increases of the oscillation frequency are limited by the OF level experimentally (which is mainly determined by the attenuation in the external cavity), the frequency modulation property is clearly observed. The tuning range of the OF level from the polarizer matches well with the simulated tuning range of κ [around ~ 1.3 dB in Fig. 8(a), ~ 1.0 dB in Fig. 8(b), and ~ 2.0 dB in Fig. 8(c)]. These results demonstrate we can estimate quite accurately the external cavity parameters based on the oscillation frequency of the feedback dynamics.

IV. CONCLUSION

In conclusion, we observed feedback dynamics in single-mode THz QCLs, which exhibits various wave forms

depending on the feedback phase and has frequency modulation properties. Because semiconductor lasers obey the same excess frequency equation, the TIs appear to be a universal phenomenon and exist in other semiconductor lasers under different OF conditions. For example, the TIs around f_{EC} exist and modulate relaxation oscillations in LDs when they are operating in the long cavity regime (frequency splitting regime) [21]. When LDs are operating in the short cavity regime, the regular pulse packages are also composed of TI dynamics around f_{EC} [5]. The TIs observed here are important when the THz QCL is operated in pulsed mode with pulses up to the order of hundreds of nanoseconds, as they will appear as a noticeable part of the signal. Moreover, as the frequency of

the TIs is principally determined by the external cavity length, these TIs provide a pathway to a THz sensing and imaging modality.

ACKNOWLEDGMENTS

We acknowledge support from: the Australian Research Council Discovery Project (Grants No. DP200101948); and the Engineering and Physical Sciences Research Council (EPSRC UK) through Grants No. EP/J002356/1, No. EP/P021859/1, and No. EP/T034246/1. X.Q. acknowledges support under Advance Queensland Industry Research Fellowships program.

-
- [1] R. Tkach and A. R. Chraplyvy, Regimes of feedback effects in 1.5- μm distributed feedback lasers, *J. Lightwave Technol.* **4**, 1655 (1986).
- [2] S. Donati and R.-H. Horng, The diagram of feedback regimes revisited, *IEEE J. Sel. Top. Quantum Electron.* **19**, 1500309 (2013).
- [3] L. Jumpertz, *Nonlinear Photonics in Mid-infrared Quantum Cascade Lasers* (Springer International Publishing AG, Cham, Switzerland, 2017), Chap. 3.
- [4] T. Erneux, A. Gavrielides, and M. Sciamanna, Stable microwave oscillations due to external-cavity-mode beating in laser diodes subject to optical feedback, *Phys. Rev. A* **66**, 033809 (2002).
- [5] T. Heil, I. Fischer, W. Elsässer, and A. Gavrielides, Dynamics of Semiconductor Lasers Subject to Delayed Optical Feedback: The Short Cavity Regime, *Phys. Rev. Lett.* **87**, 243901 (2001).
- [6] F. P. Mezzapesa, L. L. Columbo, M. Brambilla, M. Dabbicco, S. Borri, M. S. Vitiello, H. E. Beere, D. A. Ritchie, and G. Scamarcio, Intrinsic stability of quantum cascade lasers against optical feedback, *Opt. Express* **21**, 13748 (2013).
- [7] L. L. Columbo and M. Brambilla, Multimode regimes in quantum cascade lasers with optical feedback, *Opt. Express* **22**, 10105 (2014).
- [8] L. Jumpertz, M. Carras, K. Schires, and F. Grillot, Regimes of external optical feedback in 5.6 μm distributed feedback mid-infrared quantum cascade lasers, *Appl. Phys. Lett.* **105**, 131112 (2014).
- [9] L. Jumpertz, K. Schires, M. Carras, M. Sciamanna, and F. Grillot, Chaotic light at mid-infrared wavelength, *Light Sci. Appl.* **5**, e16088 (2016).
- [10] L. Weicker, D. Wolfersberger, and M. Sciamanna, Stability analysis of a quantum cascade laser subject to phase-conjugate feedback, *Phys. Rev. E* **98**, 012214 (2018).
- [11] N. N. Vukovic, J. V. Radovanovic, V. B. Milanovic, A. V. Antonov, D. I. Kuritsyn, V. V. Vaks, and D. L. Boiko, Numerical study of Risken–Nummedal–Graham–Haken instability in mid-infrared Fabry–Pérot quantum cascade lasers, *Opt. Quantum Electron.* **52**, 91 (2020).
- [12] H. Hübers, H. Richter, R. Eichholz, M. Wienold, K. Biermann, L. Schrottke, and H. T. Grahn, Heterodyne spectroscopy of frequency instabilities in terahertz quantum-cascade lasers induced by optical feedback, *IEEE J. Sel. Top. Quantum Electron.* **23**, 1800306 (2017).
- [13] Y. L. Lim, K. Bertling, T. Taimre, T. Gillespie, C. Glenn, A. Robinson, D. Indjin, Y. Han, L. Li, E. H. Linfield, A. G. Davies, P. Dean, and A. D. Rakić, Coherent imaging using laser feedback interferometry with pulsed-mode terahertz quantum cascade lasers, *Opt. Express* **27**, 10221 (2019).
- [14] A. D. Rakić, T. Taimre, K. Bertling, Y. L. Lim, P. Dean, D. Indjin, Z. Ikonić, P. Harrison, A. Valavanis, S. P. Khanna, M. Lachab, S. J. Wilson, E. H. Linfield, and A. G. Davies, Swept-frequency feedback interferometry using terahertz frequency QCLs: A method for imaging and materials analysis, *Opt. Express* **21**, 22194 (2013).
- [15] G. Agnew, A. Grier, T. Taimre, Y. L. Lim, K. Bertling, Z. Ikonić, A. Valavanis, P. Dean, J. Cooper, S. P. Khanna, M. Lachab, E. H. Linfield, A. G. Davies, P. Harrison, D. Indjin, and A. D. Rakić, Model for a pulsed terahertz quantum cascade laser under optical feedback, *Opt. Express* **24**, 20554 (2016).
- [16] S. Barbieri, J. Alton, H. E. Beere, J. Fowler, E. H. Linfield, and D. A. Ritchie, 2.9 THz quantum cascade lasers operating up to 70 K in continuous wave, *Appl. Phys. Lett.* **85**, 1674 (2004).
- [17] M. Wienold, L. Schrottke, M. Giehler, R. Hey, W. Anders, and H. T. Grahn, Low-voltage terahertz quantum-cascade lasers based on LO-phonon-assisted interminiband transitions, *Electron. Lett.* **45**, 1030 (2009).
- [18] A. D. Rakić, T. Taimre, K. Bertling, Y. L. Lim, P. Dean, A. Valavanis, and A. D. Rakić, Sensing and imaging using laser feedback interferometry with quantum cascade lasers, *Appl. Phys. Rev.* **6**, 021320 (2019).
- [19] R. Kliese, T. Taimre, A. A. A. Bakar, Y. L. Lim, K. Bertling, M. Nikolić, J. Perchoux, T. Bosch, and A. D. Rakić, Solving self-mixing equations for arbitrary feedback levels: A concise algorithm, *Appl. Opt.* **53**, 3723 (2014).
- [20] G. Agnew, A. Grier, T. Taimre, K. Bertling, Y. L. Lim, Z. Ikonić, A. Valavanis, D. Indjin, and A. D. Rakić, Frequency tuning range in pulsed terahertz quantum cascade lasers: Applications in interferometry, *IEEE J. Quantum Electron.* **54**, 2300108 (2018).
- [21] N. A. Olsson and W. T. Tsang, Transient effects in external cavity semiconductor lasers, *IEEE J. Quantum Electron.* **QE-19**, 1479 (1983).